J. Phys.: Condens. Matter **9** (1997) 7039–7061. Printed in the UK PII: S0953-8984(97)80552-8

Tunnelling in the nonintegrable trimer—a step towards quantum breathers

S Flach† and V Fleurov‡

† Max-Planck-Institut für Physik Komplexer Systeme, Nöthnitzer Strasse 38, D-01187 Dresden, Germany

‡ School of Physics and Astronomy, Raymond and Beverly Sackler Faculty of Exact Sciences, Tel Aviv University, Tel Aviv, 69978, Israel

Received 2 January 1997, in final form 14 March 1997

Abstract. We analyse the classical and quantum properties of the nonintegrable trimer problem. The Hamiltonian exhibits permutation symmetry. A single parameter tunes the distance of the system from the integrable dimer. There exist classical trajectories—both regular and chaotic—which are not invariant under permutation. We numerically diagonalize the quantum Hamiltonian and investigate properties of pairs of tunnelling eigenstates, and compare to the corresponding classical phase-space properties. Tunnelling states survive avoided crossings with other states, and continue to exist as long as the classical phase space supports regular islands. We relate these findings to the problem of quantum breathers and single-bond excitations in molecules.

1. Introduction

The motivation for the present work arises from efforts to quantize discrete breathers. Discrete breathers are time-periodic spatially localized solutions of equations describing classical degrees of freedom (DOF) arranged on a Hamiltonian lattice (think of atom vibrations in a crystal). For a history of the subject see [1, 2] and [3]. Recently progress in the understanding of the existence and properties of discrete breathers has been achieved [4–12]. The Hamiltonian governing the equations of motion is invariant under discrete translational symmetry. Discrete breather solutions are periodic orbits which are not invariant under the discrete translational symmetry. They are structurally stable and exist independently of the lattice dimension [8, 9]. Discrete breathers can exist because of a combination of two effects—the discreteness of the system and the nonlinearity in the equations of motion. The discreteness provides finite bounds to the frequency spectrum (phonon spectrum) of the linearized equations of motion. The nonlinearity allows for frequencies outside the phonon spectrum. Thus the necessary condition for the existence of discrete breathers—that all multiples of the breather frequency have to be outside the phonon spectrum—can be fulfilled in principle [7].

A natural question is then what remains of discrete breathers if the corresponding quantum problem is considered. Since the Schrödinger equation is linear and translationally invariant, all eigenstates must obey the Bloch theorem. Thus we cannot expect eigenstates of the Hamiltonian to be spatially localized (on the lattice). On the other hand, the question of the correspondence between the quantum eigenvalue problem and the classical dynamical evolution needs an answer.

0953-8984/97/337039+23$19.50

The concept of tunnelling is a possible answer to this puzzle. Naively speaking, we quantize the family of periodic orbits associated with a discrete breather located somewhere on the lattice. Notice that there are as many such families as there are lattice sites. The quantization (e.g. Bohr–Sommerfeld) yields some eigenvalues [13]. Since we can perform the same procedure with any family of discrete breather periodic orbits which differ only in their location on the lattice, we obtain N-fold degeneracy for every eigenvalue thus obtained, where N stands for the number of lattice sites. Unless we consider the trivial case of, say, uncoupled lattice sites, these degeneracies will be lifted. Consequently, we will instead obtain bands of states with finite bandwidth which can even hybridize with other states. These bands will be called quantum breather bands. The inverse tunnelling time of a semiclassical breather from one site to a neighbouring one is a measure of the bandwidth.

We can then formulate the following expectation: if a classical nonlinear Hamiltonian lattice possesses discrete breathers, its quantum counterpart should show up with nearly degenerate bands of eigenstates, if the classical limit is considered. The number of states in such a band is N, and the eigenfunctions are given by Bloch-like superpositions of the semiclassical eigenfunctions obtained using the above-mentioned Bohr–Sommerfeld quantization of the classical periodic orbits. By 'nearly degenerate', we mean that the spacing between different breather bands is much larger than each bandwidth, and the classical limit implies large eigenvalues.

Another property of a quantum breather state is that such a state shows up with exponential localization in appropriate correlation functions [14]. This approach selects all particle-like states, no matter how deep one is in the quantum regime. In this sense quantum breather states belong to the class of particle-like bound states.

Intuitively it is evident that, for large energies and N, the density of states becomes large too. What will happen to the expected quantum breather bands then? Will the hybridization with other nonbreather states destroy the particle-like nature of the quantum breather, or not? What is the impact of the nonintegrability of most systems allowing for classical breather solutions? Since the quantum case corresponds to a quantization of the classical phase space, we could expect that chaotic trajectories lying near to classical breather solutions might affect the corresponding quantum eigenstates.

Quantum breather states have been so far obtained numerically for small one-dimensional systems ($N \leqslant 8$) [14–16]. An exception is the discrete nonlinear Schrödinger equation, where bound states of two bosons can be in principle obtained analytically for any system size [17]. Naturally, the corresponding states are low-energy states. The questions from the preceding paragraph are still to be answered.

Properties of high-energy states can be studied much more easily for systems with small N. A series of papers were devoted to the properties of the quantum dimer [18–20]. This system to be introduced in the next section describes the dynamics of bosons fluctuating between two sites. The number of bosons is conserved, and, taken together with the conservation of energy, this means that the system appears to be integrable. Of course, one cannot consider spatial localization in such a model. However, a reduced form of the discrete translational symmetry—namely the permutational symmetry of the two sites—can be imposed. Together with the addition of nonlinear terms in the classical equations of motion, the dimer allows for classical trajectories which are not invariant under permutation [21]. The phase space can be completely analysed; all isolated periodic orbits can be found. There appears exactly one bifurcation on one family of isolated periodic orbits, which leads to the appearance of a separatrix in phase space. The separatrix separates three regions—one invariant and two noninvariant under permutations. The subsequent analysis of the quantum dimer demonstrated the existence of pairs of eigenstates with nearly equal

eigenenergies [18]. The separatrix and the bifurcation in the classical phase space can be traced in the spectrum of the quantum dimer [20].

The integrability of the dimer does not allow for a study of the influence of chaos on the tunnelling properties of the above-mentioned pairs of eigenstates. A natural extension of the dimer to a trimer adds a third degree of freedom without adding a new integral of motion. Consequently the trimer is nonintegrable [22]. So far, the quantum trimer has only been studied with respect to universal properties of the eigenvalue spectrum [23–26], and mean-field approaches have been analysed in [27]. A comparatively simple numerical quantization of the trimer will allow us to study the behaviour of many tunnelling states in the large-energy domain of the eigenvalue spectrum. Note that the trimer considered below will be slightly different from the one analysed in [22–27].

2. The dimer

Here we will briefly review the relevant results† for the integrable dimer with Hamiltonian

$$H = \frac{1}{2}(P_1^2 + P_2^2 + X_1^2 + X_2^2) + \frac{1}{8}((P_1^2 + X_1^2)^2 + (P_2^2 + X_2^2)^2) + \frac{C}{2}(X_1X_2 + P_1P_2). \quad (2.1)$$

$P_{1,2}$, $X_{1,2}$ are the canonically conjugate momenta and positions of two degrees of freedom. The system (2.1) is integrable, because the classical Poisson bracket of

$$B = P_1^2 + P_2^2 + X_1^2 + X_2^2 \quad (2.2)$$

with H vanishes. Furthermore, equation (2.1) is invariant under the permutation of the indices $1 \leftrightarrow 2$.

2.1. Classical properties

Substituting $\Psi = (1/\sqrt{2})(X + \mathrm{i}P)$, equation (2.1) becomes

$$H = \Psi_1^*\Psi_1 + \Psi_2^*\Psi_2 + \frac{1}{2}((\Psi_1^*\Psi_1)^2 + (\Psi_2^*\Psi_2)^2) + C(\Psi_1^*\Psi_2 + \Psi_2^*\Psi_1) \quad (2.3)$$

with the equations of motion $\dot{\Psi}_{1,2} = \mathrm{i}\,\partial H/\partial\Psi_{1,2}^*$.

Isolated periodic orbits (IPOs) satisfy the relation $\boldsymbol{\nabla H} \| \boldsymbol{\nabla B}$. Let us parametrize the phase space of (2.3) with $\Psi_{1,2} = A_{1,2}\mathrm{e}^{\mathrm{i}\phi_{1,2}}$, $A_{1,2} \geqslant 0$. It follows that $A_{1,2}$ is time independent, and $\phi_1 = \phi_2 + \Delta$ with $\Delta = 0, \pi$ and $\dot{\phi}_{1,2} = \omega$ also time independent. Solving the algebraic equations for the amplitudes of the IPOs we obtain

$$\text{I:} \qquad A_{1,2}^2 = \frac{1}{2}B \qquad \Delta = 0 \qquad \omega = 1 + C + \frac{1}{2}B \quad (2.4)$$

$$\text{II:} \qquad A_{1,2}^2 = \frac{1}{2}B \qquad \Delta = \pi \qquad \omega = 1 - C + \frac{1}{2}B \quad (2.5)$$

$$\text{III:} \qquad A_1^2 = \frac{1}{2}B(1 \pm \sqrt{1 - 4C^2/B^2}) \qquad \Delta = 0 \qquad \omega = 1 + B. \quad (2.6)$$

IPO III corresponds to two elliptic solutions which break the permutational symmetry. IPO III exists for $B \geqslant B_b$ with $B_b = 2C$ and occurs through a bifurcation from IPO I [21]. The corresponding separatrix manifold is uniquely defined by the energy of IPO I at a given value of $B \geqslant B_b$. This manifold separates three regions in phase space—two with symmetry-broken solutions, each one containing one of the IPOs III, and one with symmetry-conserving solutions containing the elliptic solution IPO II. The separatrix manifold itself

† We follow closely the explanations in [20].

contains the hyperbolic IPO I. For $B \leqslant B_b$ only two IPOs exist—IPO I and IPO II, both of them being of elliptic character. Remarkably, there exist no other IPOs, and the above-mentioned bifurcation and separatrix manifolds are the only ones present in the classical phase space of (2.1) [21].

To conclude the analysis of the classical part, we list the energy properties of the different phase-space parts separated by the separatrix manifold. First, it is straightforward to show that the IPOs (2.4)–(2.6) correspond to maxima, minima or saddle points of the energy in the allowed energy interval for a given value of B, with no other extrema or saddle points present [21]. It follows that

$$E_1 = H(\text{IPO I}) = B + \frac{1}{4}B^2 + CB \tag{2.7}$$

$$E_2 = H(\text{IPO II}) = B + \frac{1}{4}B^2 - CB \tag{2.8}$$

$$E_3 = H(\text{IPO III}) = B + \frac{1}{2}B^2 + C^2. \tag{2.9}$$

For $B < B_b$ we have $E_1 > E_2$ (IPO I—maximum, IPO II—minimum). For $B \geqslant B_b$ it follows that $E_3 > E_1 > E_2$ (IPO III—maximum, IPO I—saddle, IPO II—minimum). If $B < B_b$, then all trajectories are symmetry conserving. If $B \geqslant B_b$, then trajectories with energies $E_1 < E \leqslant E_3$ are symmetry breaking, and trajectories with $E_2 \leqslant E \leqslant E_1$ are symmetry conserving.

2.2. Quantum properties

The quantum eigenvalue problem can be properly analysed in second quantization, which amounts to replacing the complex functions Ψ, Ψ^* in (2.3) by the boson annihilation and creation operators a, a^+ with the standard commutation relations (to enforce the invariance under the exchange $\Psi \Leftrightarrow \Psi^*$, the substitution has to be done on rewriting $\Psi\Psi^* = (1/2)(\Psi\Psi^* + \Psi^*\Psi)$):

$$H = \frac{5}{4} + \frac{3}{2}(a_1^+ a_1 + a_2^+ a_2) + \frac{1}{2}((a_1^+ a_1)^2 + (a_2^+ a_2)^2) + C(a_1^+ a_2 + a_2^+ a_1). \tag{2.10}$$

Note that $\hbar = 1$ here, so the eigenvalues b of $B = a_1^+ a_1 + a_2^+ a_2$ are integers. Since B commutes with H, we can diagonalize the Hamiltonian in the basis of eigenfunctions of B. Each value of b corresponds to a subspace of the dimension $b + 1$ in the space of eigenfunctions of B. These eigenfunctions are products of the number states $|n\rangle$ of each degree of freedom, and can be characterized by a symbol $|n, m\rangle$ with n bosons in the site 1 and m bosons in the site 2. For a given value of b it follows that $m = b - n$. So we can actually label each state with just one number n: $|n, (b-n)\rangle \equiv |n)$. Consequently the eigenvalue problem at fixed b amounts to diagonalizing the matrix

$$H_{nm} = \begin{cases} \dfrac{5}{4} + \dfrac{3}{2}b + \dfrac{1}{2}(n^2 + (b-n)^2) & n = m \\ C\sqrt{n(b+1-n)} & n = m+1 \\ C\sqrt{(n+1)(b-n)} & n = m-1 \\ 0 & \text{otherwise} \end{cases} \tag{2.11}$$

where $n, m = 0, 1, 2, \ldots, b$. Notice that the matrix H_{nm} is a symmetric band matrix. The additional symmetry $H_{nm} = H_{(b-n),(b-m)}$ is a consequence of the permutational symmetry of H.

For $C = 0$, the matrix H_{nm} is diagonal, with the property that each eigenvalue is doubly degenerate (except for the state $|b/2)$ for the even values of b). The classical phase space contains only symmetry-broken trajectories, with the exception of IPO II and the separatrix with IPO I (in fact in this limit the separatrix manifold is nothing but a resonant torus containing both IPOs I and II). So with the exception of the separatrix manifold, all tori break permutational symmetry and come in two groups separated by the separatrix. Then quantizing each group will lead to pairs of degenerate eigenvalues—one from each group. There is a clear correspondence to the spectrum of the diagonal ($C = 0$) matrix H_{nm}. The eigenvalues $H_{00} = H_{bb}$ correspond to the quantized IPOs III. With increasing n the eigenvalues $H_{nn} = H_{(b-n),(b-n)}$ correspond to quantized tori further away from the IPO III. Finally, the states with $n = b/2$ for even b or $n = (b-1)/2$ for odd b are the tori that are closest to the separatrix. Switching the side diagonals on by increasing C will lead to a splitting of all pairs of eigenvalues. In the case of small values of b, these splittings have no correspondence to classical system properties. However, in the limit of large b, we enter the semiclassical regime, and, due to the integrability of the system, eigenfunctions should correspond to tori in the classical phase space which satisfy the Einstein–Brillouin–Keller quantization rules [28].

Increasing C from zero will lead to a splitting ΔE_n of the eigenvalue doublets of $C = 0$. In other words we find pairs of eigenvalues, which are related to each other through the symmetry of their eigenvectors and (for small enough C) through the small value of the splitting. These splittings have been calculated numerically and using perturbation theory [20]†. In the limit of large b, the splittings are exponentially small for energies above the classical separatrix energy (i.e. for classical trajectories which are not invariant under permutation). If the eigenenergies are lowered below the classical separatrix energy, the splittings grow rapidly up to the mean level spacing.

3. The trimer

The results from the preceding section demonstrate that the existence of classical phase-space parts with trajectories not invariant under permutation symmetry leads to exponentially weakly split pairs of eigenenergies of the corresponding Schrödinger problem. One could conclude then that nothing else should be expected for the case of a lattice—except that the number of nearly degenerate states increases, and bands are formed in the limit of an infinite lattice [34]. However, on increasing the size of the system we will certainly lose integrability (at least in most of the cases). This will in general lead to the appearance of states which are not obtainable with EBK methods, i.e. states which correspond to mixed or chaotic classical phase-space parts. The eigenenergies of these states can come close to the pairs considered. What is the impact of the interaction of these states? Will the tunnelling pair eventually be forced to increase its splitting to the mean level spacing?

The previous paragraph suggests that we are entering an area of quantum chaos for the description of which the term ‘chaos-assisted tunnelling’ has been coined [35]. Indeed there have been several publications which study the details of the splitting values as a function of the mixed classical phase-space properties [36–39]. Most of these studies test splittings which are orders of magnitude smaller than the mean level spacing. Here we will be interested in the transition from small splittings to splittings of the order of the mean level spacing [40]. For most applications this transition is the essential one, since it will signal the merging of separated timescales and energy scales.

† See [29–33] for more results on multidimensional tunnelling.

3.1. Description of the model

Consider the Hamiltonian of a trimer

$$H = \frac{1}{2}(P_1^2 + P_2^2 + P_3^2 + X_1^2 + X_2^2 + X_3^2) + \frac{1}{8}[(P_1^2 + X_2^2)^2 + (P_1^2 + X_2^2)^2] + \frac{C}{2}(X_1X_2 + P_1P_2) + \frac{\delta}{2}(X_1X_3 + P_1P_3 + X_2X_3 + P_2P_3). \tag{3.1}$$

Its part depending on the first two coordinates $X_{1,2}$ and momenta $P_{1,2}$ is just the dimer whose properties were briefly reviewed in the previous section. The additional degree of freedom is described by the canonically conjugate coordinates X_3 and P_3, and the coupling to the dimer is controlled by the parameter δ. Similarly to the dimer, the trimer (3.1) conserves the norm

$$B = P_1^2 + P_2^2 + P_3^2 + X_1^2 + X_2^2 + X_3^2. \tag{3.2}$$

The system is nonintegrable for $\delta \neq 0$. Exceptions are the case where $\delta = 0$ and maybe some other nonzero values of δ which we, however, did not encounter. The parameter δ will be used as a measure of nonintegrability of our system.

Model (3.1) is invariant under the permutation of the indices $1 \leftrightarrow 2$. We will label the corresponding permutation operator $\hat{P}_c$ acting on the classical phase space, and $\hat{P}_q$ acting on the quantum Hilbert space.

Using the transformation $\Psi_i = (1/\sqrt{2})(X_i + \mathrm{i}P_i)$, equation (3.1) becomes

$$H = \Psi_1^*\Psi_1 + \Psi_2^*\Psi_2 + \Psi_3^*\Psi_3 + \frac{1}{2}[(\Psi_1^*\Psi_1)^2 + (\Psi_2^*\Psi_2)^2] + C(\Psi_1^*\Psi_2 + \Psi_2^*\Psi_1) + \delta(\Psi_1^*\Psi_3 + \Psi_3^*\Psi_1 + \Psi_2^*\Psi_3 + \Psi_3^*\Psi_2). \tag{3.3}$$

A property of (3.3) is its scale invariance. Given an energy E, parameters C, δ, and initial conditions Ψ_i, we can generate a trajectory $\Psi_i(t)$. This trajectory is found for the energy E/B^2, parameters $C/B, \delta/B$, and initial conditions Ψ_i/B, and is given by $\Psi_i(t/B)/B$. Consequently we can always choose $B = 1$, and are left with two independent system parameters C, δ.

3.2. Classical properties of the trimer

Parametrizing the phase space of Hamiltonian (3.1) with

$$\Psi_i = A_i \mathrm{e}^{\mathrm{i}\varphi_i}$$

we obtain

$$H = A_1^2 + A_2^2 + A_3^2 + \frac{1}{2}(A_1^4 + A_2^4) + 2CA_1A_2\cos\Delta_{12} + 2\delta A_3(A_1\cos\Delta_{13} + A_2\cos\Delta_{23}) \tag{3.4}$$

where $\Delta_{ij} = \varphi_i - \varphi_j$. As in the case of the dimer, isolated periodic orbits can be found using the relation $\boldsymbol{\nabla H} \| \boldsymbol{\nabla B}$ [20]. Note, however, that, contrary to the case for the integrable dimer, this condition is necessary but not sufficient for the nonintegrable trimer. Thus we cannot obtain all isolated periodic orbits. The ones which can be found satisfy the condition $\Delta_{ij} = 0, \pi$ on the phases, and

$$\begin{aligned} &2A_1 + 2A_1^3 + 2CA_2\cos\Delta_{12} + 2\delta A_3\cos\Delta_{13} = 2(\kappa+1)A_1 \\ &2A_2 + 2A_2^3 + 2CA_1\cos\Delta_{12} + 2\delta A_3\cos\Delta_{23} = 2(\kappa+1)A_2 \\ &2A_3 + 2\delta(A_1\cos\Delta_{13} + A_2\cos\Delta_{23}) = 2(\kappa+1)A_3. \end{aligned} \tag{3.5}$$

Here the eigenvalue κ is to be determined.

With the allowed values of the phase differences we arrive at the equations

$$A_2 = \pm\left(\frac{\beta}{\alpha}A_1 - \frac{1}{\alpha}A_1^3\right) \tag{3.6}$$

$$A_1 = \pm\left(\frac{\beta}{\alpha}A_2 - \frac{1}{\alpha}A_2^3\right) \tag{3.7}$$

where $\alpha = C + \delta^2/\kappa$ and $\beta = \kappa - \delta^2/\kappa$. The remaining value of A_3 can be found with the help of (3.5). We have to consider four situations corresponding to four possible sets of the allowed phase difference $\Delta_{12}, \Delta_{13}, \Delta_{23}$. These are: $(0, 0, 0)$ and $(0, \pi, \pi)$ (plus, in equations (3.6) and (3.7)); and $(\pi, \pi, 0)$ and $(\pi, 0, \pi)$ (minus, in equations (3.6) and (3.7)).

The results for all orbits found are given in table 1.

Table 1. Results for orbits.

IPO No	A_1^2	A_2^2	$(\Delta_{12}, \Delta_{13}, \Delta_{23})$	Conditions
1	$\beta - \alpha$	$\beta - \alpha$	(0, 0, 0)	$\alpha > 0$ $\beta > \alpha$
2	$\beta + \alpha$	$\beta + \alpha$	$(\pi, 0, \pi)$ $(\pi, \pi, 0)$	$\kappa > -C$
3	$\frac{1}{2}[\beta \pm \sqrt{\beta^2 - 4\alpha^2}]$	$\frac{1}{2}[\beta \mp \sqrt{\beta^2 - 4\alpha^2}]$	(0, 0, 0)	$\alpha > 0$ $\beta > \alpha$ $\kappa > C(1 + \sqrt{1 + 3\delta^2/C^2})$
4	$\beta - \alpha$	$\beta - \alpha$	$(0, \pi, \pi)$	$\delta < C$ $\mathrm{Max}[-\delta; \frac{1}{2}(C - \sqrt{C^2 + 8\delta^2})] < \kappa < 0$
5	$\frac{1}{2}[\beta \pm \sqrt{\beta^2 - 4\alpha^2}]$	$\frac{1}{2}[\beta \mp \sqrt{\beta^2 - 4\alpha^2}]$	$(0, \pi, \pi)$	$\delta < C$ $C(1 - \sqrt{1 + 3\delta^2/C^2}) < \kappa < \delta^2/C$
6	$\frac{1}{2}[\beta \pm \sqrt{\beta^2 - 4\alpha^2}]$	$\frac{1}{2}[\beta \mp \sqrt{\beta^2 - 4\alpha^2}]$	$(\pi, \pi, 0)$ $(\pi, 0, \pi)$	$\delta < C$ $-\delta^2/C < \kappa < -C + \sqrt{C^2 - \delta^2}$

Only a few details of the list in table 1 are of importance for us. First we note that the IPO3 bifurcate from IPO1 as in the case of the dimer. However, the limit $\delta \to 0$ does not coincide with the integrable case $\delta = 0$, since then the phase space disintegrates into a continuum of dimer subspaces with different values of B, accompanied by the phase-space part of the redundant third-harmonic degree of freedom. Each subspace can contain a bifurcation; thus we find a continuum of bifurcations. For any $\delta \neq 0$, we find at most one bifurcation related to the appearance of IPO3. In terms of energy, the situation is similar to that of the dimer. If the IPO3 exist, then their energies are the largest possible for given other parameters (including B). In this case the separatrix energy of IPO1 separates two phase-space parts. The one with higher energies always contains trajectories which are not invariant under the permutation $1 \leftrightarrow 2$. In contrast to the case for the dimer, for energies lower than the separatrix energy we can still find trimer trajectories not invariant under permutation. The bifurcation IPO1–IPO3 is given by a line in the parameter space $(C; \delta)$ which cuts the axes at $(0.5; 0)$ and $(0; 3\sqrt{3}/10)$ (see figure 1). All points below this curve correspond to cases with existing orbits IPO3, whereas no IPO3 orbits exist above the curve

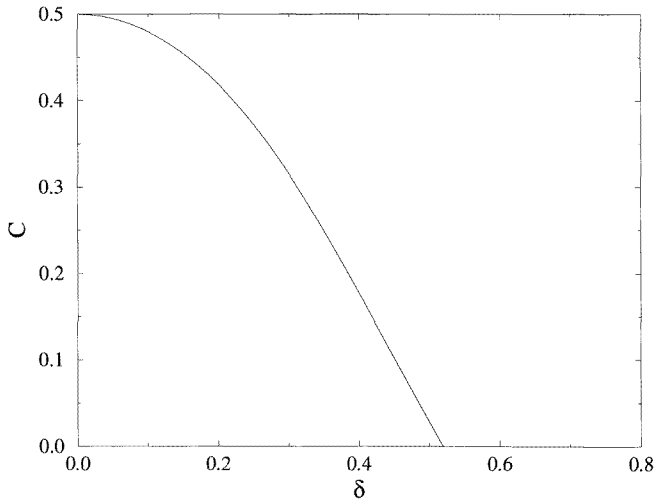

Figure 1. The bifurcation line of IPO1 in the classical trimer model with $B = 1$.

in figure 1 . This curve can be generated using $B = 1$ and the solution for IPO1 with the value of κ at the bifurcation $\kappa^b = C(1 + \sqrt{1 + 3\delta^2/C^2})$.

The remaining bifurcations which follow from the list in table 1 are low-energy ones, well separated from the bifurcation in which we are interested. Thus we will not consider these additional bifurcations further.

Since we are interested in studying the influence of nonintegrability ($\delta \neq 0$), we need to define an appropriate region in the control parameter space $(C; \delta)$. This region should stay below the bifurcation line in figure 1 and sufficiently far from it. We choose $C = 0.05$. We have to be sure that essential parts of the classical phase space become chaotic for values of δ much smaller than 0.5 (see figure 1). We used Poincaré maps to study the phase-space properties of the system. As expected, for $\delta = 10^{-6}$ the system is close to an integrable limit, and for all allowed energies the motion is practically quasiperiodic. However, for the value $\delta = 0.1$, most of the phase-space parts (especially close to the separatrix containing IPO1) are already chaotic. Still, $(C; \delta) = (0.05; 0.1)$ is sufficiently far from the bifurcation line in figure 1. Thus we can be sure that changes in the energy splittings of the corresponding quantum problem on the stripe $C = 0.05; 0 < \delta < 0.1$ are not due to the disappearance of the classical phase-space parts with broken symmetry. The main effect, if any, will stem from the chaotization of the classical phase space.

3.3. Quantum trimer properties

Similarly to the dimer, the quantum trimer Hamiltonian is represented in the form

$$H = \frac{15}{8} + \frac{3}{2}(a_1^+ a_1 + a_2^+ a_2 + a_3^+ a_3) + \frac{1}{2}\left[(a_1^+ a_1)^2 + (a_2^+ a_2)^2\right] + C(a_1^+ a_2 + a_2^+ a_1) + \delta(a_1^+ a_3 + a_3^+ a_1 + a_2^+ a_3 + a_3^+ a_2). \tag{3.8}$$

Again, $B = a_1^+ a_1 + a_2^+ a_2 + a_3^+ a_3$ commutes with the Hamiltonian, and thus we can diagonalize (3.8) in the basis of eigenfunctions of B. For any finite eigenvalue b of B, the number of states is finite, namely $(b + 1)(b + 2)/2$. Thus the infinite-dimensional Hilbert space separates into an infinite set of finite-dimensional subspaces, each subspace containing

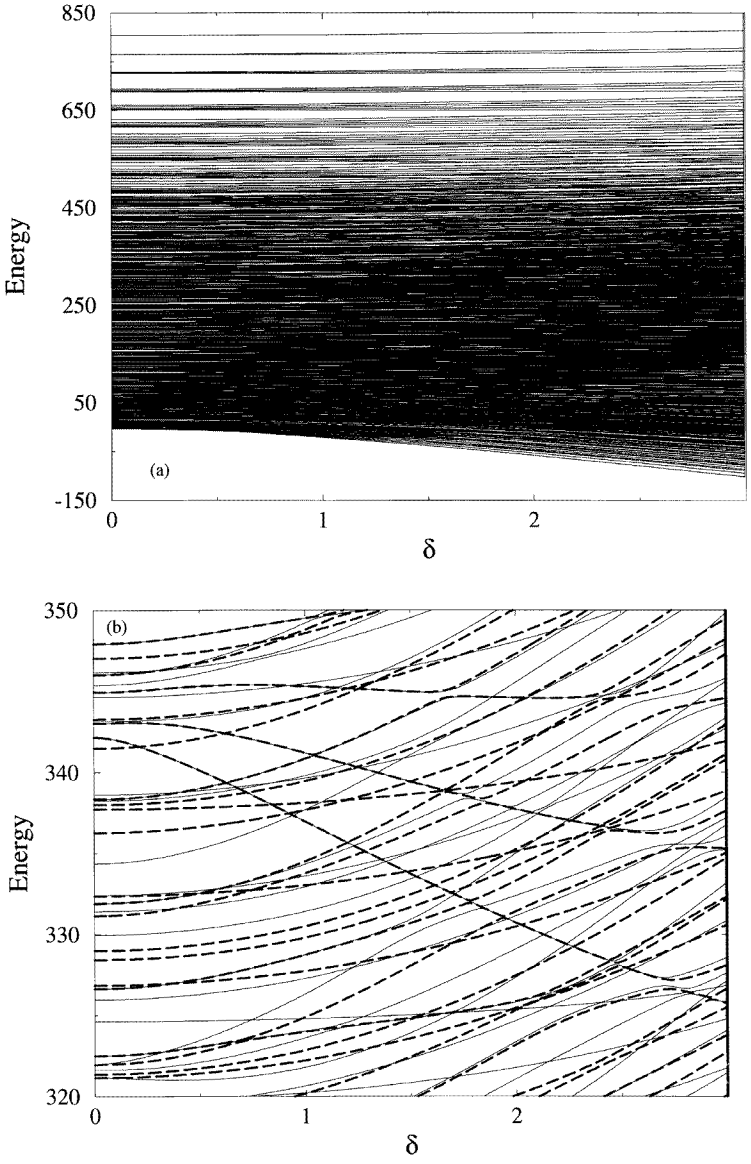

Figure 2. Eigenenergies of the quantum trimer with $b = 40$ and $C = 2$. Lines connect data points for a given state. (a) The full spectrum; (b) an area of (a) shown with an enlarged energy scale. Solid lines—symmetric eigenstates; thick dashed lines—antisymmetric eigenstates.

only vectors with a given eigenvalue b. These eigenfunctions are products of the number states $|n\rangle$ of each degree of freedom, and can be characterized by a symbol $|n, m, l\rangle$ where we have n bosons on site 1, m bosons on site 2, and l bosons on site 3. For a given value b, it follows that $l = b - m - n$. So we can actually label each state with just two numbers (n, m): $|n, m, (b - n - m)\rangle \equiv |n, m\rangle$.

The matrix elements of (3.8) connecting states from different b-subspaces vanish. Thus for any given b the task amounts to diagonalizing a finite-dimensional matrix. The matrix

has a tridiagonal block structure, with each diagonal block being a dimer matrix (2.11). The nonzero off-diagonal blocks contain interaction terms proportional to δ. Since H commutes with $\hat{P}_q$, we consider symmetric $|\Psi\rangle_s$ and antisymmetric $|\Psi\rangle_a$ states. The structure of the corresponding symmetric and antisymmetric decompositions of H is similar to that of H itself.

In the following, we will present results for $b = 40$. We will also drop the first two terms of the rhs in (3.8), because these only lead to a shift of the energy spectrum. Since we evaluate the matrix elements explicitly, we need only a few seconds to obtain all eigenvalues and eigenvectors with the help of standard Fortran routines. In figure 2(a) we plot the eigenenergies as a function of δ for $C = 2$. As discussed above, the Hamilton matrix decomposes into noninteracting blocks for $\delta = 0$, each block corresponding to a dimer with a boson number between 0 and b. For $\delta \neq 0$ the nonzero block–block interaction leads to typical features in the spectrum, like, e.g., avoided crossings observable in the enlargement shown as figure 2(b). From figure 2(a) we observe that the quantum energy spectrum extends roughly over 10^3, which implies an average spacing of order 10^0. Also, the upper third of the spectrum is diluted compared to the lower two thirds. The fan-like spreading of the spectrum with increasing values of δ can be qualitatively understood using recent results which interpret the dependence of eigenvalues of random matrices on a single parameter as a time evolution of a one-dimensional gas with some repulsive two-body interaction [41, 42]. Here time is equivalent to the matrix parameter (δ in our case). The edges of the spectrum correspond then to the particles located at the edge of a finite cluster. The repulsion from the cluster pushes these particles away, and thus enlarges the cluster. Of course, in our case the matrix is certainly not completely random, yet still the enlarging of the cluster is observed.

The correspondence to the classical model is obtained with the use of the transformation $E_{cl} = E_{qm}/b^2 + 1$ and for parameters C/b and δ/b (the classical value for B is $B = 1$).

In order to characterize the quantum properties it is not enough to discuss the eigenenergies. As we discussed in the introduction, the quantum breather states for lattices are expected to have particle-like properties. Consequently we have to probe the eigenfunctions of the quantum trimer problem as well. Since all eigenfunctions are symmetric or antisymmetric with respect to $\hat{P}_q$, and there is no notion of a spatial distance (like on a lattice), we can only define a measure for an eigenfunction to correspond to a classically symmetry-broken trajectory. We use the squared amplitude of the *hyperbolic part* $S_{|\Psi\rangle}$ of a given eigenfunction $|\Psi\rangle$:

$$S_{|\Psi\rangle} = \sum_n |\phi_{nn}|^2 \qquad |\Psi\rangle = \sum_{n,m} \phi_{nm}|n, m). \tag{3.9}$$

The parameter S, which by definition is in the range $0 \leqslant S \leqslant 1$, can be considered as a generalization of the value of an eigenfunction at the barrier position of a double-well potential. Note that the antisymmetric eigenfunctions of a double-well potential will have a knot at the barrier site, so, for these, $S = 0$ (in our case, $\phi_{nn} = 0$ for any antisymmetric eigenstate). However, the value of S for a symmetric eigenfunction will be of the order of the corresponding tunnelling splitting. In the classical limit, the trajectories not invariant under permutations yield $S = 0$ (no tunnelling) whereas the trajectories invariant under permutation will have nonzero S-values of the order of $1/B$.

We tested the correspondence between S and the tunnelling splittings numerically, and found excellent agreement with the above statements. In figure 3 we plot the dependence $S(E)$ for all of the symmetric eigenstates for $b = 40$, $C = 2$, and $\delta = 1$. Eigenstates with S-values of the order of $1/b$ or larger do not belong to tunnelling pairs, whereas S-values

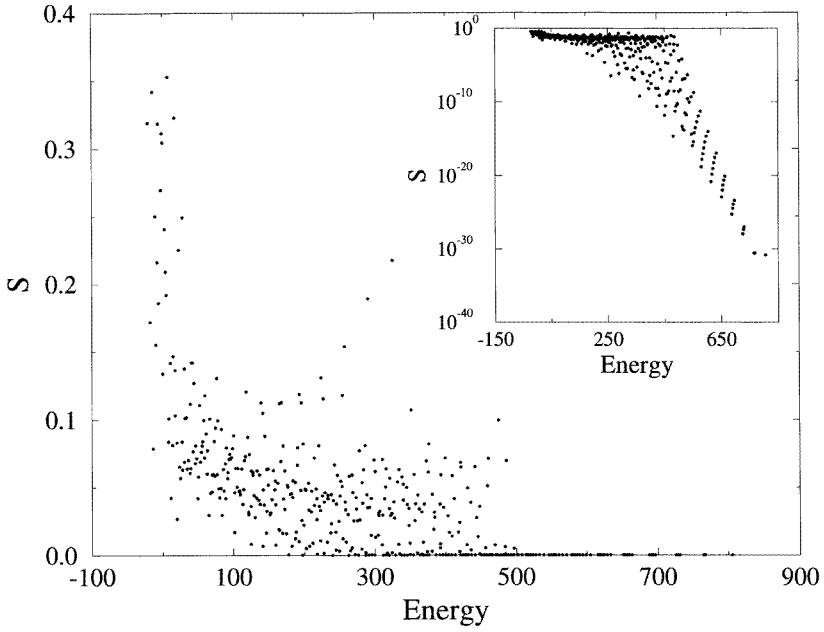

Figure 3. S versus the eigenenergy E for $b = 40$, $C = 2$, and $\delta = 1$. The inset is the same, but as a log–linear plot.

below $0.01/b$ indicate tunnelling pairs. S-values considerably larger than $1/b$ (typically $10/b$) indicate closeness to the classical separatrix, since classical trajectories will spend most of their time near the hyperbolic IPO1.

4. Properties of tunnelling pairs

In this section we will investigate the fragility of tunnelling pairs to changes in the spectrum upon variation of δ. From our numerical studies we find three essential processes.

The first one is the avoided crossing between a tunnelling pair and a single state. Since the single state has a well-defined symmetry, it is interacting only with one of the two states of the tunnelling pair. Consequently we observe the avoided crossing between two states of the same symmetry [43, 44], and an unaffected smooth change of the tunnelling state with different symmetry. On passing the avoided crossing, the tunnelling pair is essentially recovered.

The second process is the avoided crossing between two tunnelling pairs. It reduces to the simultaneous appearance of two avoided crossings of two equal-symmetry states belonging to two different tunnelling pairs. Again the two tunnelling pairs are recovered once the pair–pair avoided crossing is passed.

The third process is a destruction of a tunnelling pair. This process is similar to the first process; however, the avoided crossing turns out to be fatal for the tunnelling pair.

4.1. Pair–single-state avoided crossings

Three states participate in the first process. For definiteness, label them $p1$ (the symmetric tunnelling state), $p2$ (the antisymmetric tunnelling state), and $s3$ (the symmetric single

state). We could equally well choose the single state to be antisymmetric. The eigenenergies E_{p2} and E_{s3} can be equal for some values of δ, since the eigenstates belong to different irreducible representations. The distance $\Delta_{ac} = |E_{p1} - E_{s3}|$, however, will not vanish in general. This is due to the fact that the dimension of the subspace of all real symmetric matrices of the rank N with at least two identical eigenvalues is reduced by two compared to the dimension of all real symmetric matrices of the rank N [45]. Consequently, varying a single parameter does not result in a crossing of the degenerate subspace in general. An avoided crossing reflects closeness of the chosen path to the degenerate subspace for some value(s) of the line parameter (which is δ in our case).

First we will discuss avoided crossings where the minimum nonzero value of Δ_{ac} is small compared to the average spacing of the eigenvalues. Then the avoided crossing can be studied by means of a real symmetric 2×2 matrix. The space of these matrices is three dimensional [46], whereas the subspace of degenerate matrices is one dimensional. Neglecting total shifts of the eigenvalue spectrum, we can reduce the problem to considering a two-dimensional subspace containing a degenerate point—the so-called diabolic point [47]. Encircling the degenerate point once along a closed loop leads to a geometric phase $e^{i\pi}$ accumulated by each eigenvector (a special case of the Berry phase). Passing the degenerate point along a line is then effectively equivalent to a half-loop. The accumulated phase is $e^{i\pi/2}$, i.e. eigenvectors $|\Psi_1\rangle$ and $|\Psi_2\rangle$, before passing the degenerate point, are permuted on passing: $|\Psi_1\rangle \to |\Psi_2\rangle$ and $|\Psi_2\rangle \to -|\Psi_1\rangle$ (the sign change could be permuted).

We observed many avoided crossings of that type (see figure 2(b) for an example). The tunnelling pair recovers after the crossing. The wave functions are transported through the crossing as described above.

We also observed avoided crossings where Δ_{ac} is of the order of 20% of the averaged spacing. These cases do not allow a consideration by means of a 2×2 matrix any longer.

To associate a quantum eigenstate with its classical counterpart (a periodic orbit, a torus or simply a phase-space part) the Husimi distribution is often used. This distribution is defined in the classical phase space, and is obtained by projecting a given eigenstate onto coherent states [48]. However, here it is more convenient to make use of the fact that our local basis representation corresponds to quantized classical variables $|\Psi_i|^2$. Consequently the squared expansion coefficients $\rho(n, (b - n - m)) = |\phi_{nm}|^2$ of a given eigenstate can be considered as functions $\rho(n, m)$ on the discretized two-dimensional space, $|\Psi_1|^2 = n$ and $|\Psi_3|^2 = b - n - m$. Comparing the tunnelling states with Poincaré maps of the classical system, we conclude that tunnelling states are predominantly localized in regular parts of the classical phase space which contain symmetry-broken trajectories (see the next subsection for some examples).

4.2. Pair–pair avoided crossings

Another process that we have observed is the avoided crossing of two pairs. Since members of a pair consist of a symmetric and antisymmetric state, the pair–pair crossing amounts to two avoided crossings. Let us label the four states involved as $s1, s2$ (symmetric states from the first and second pair) and $a1, a2$ (antisymmetric states from the first and second pair). Then what we observe are two simultaneous avoided crossings—one involving the two states $s1, s2$, and another one involving the two states $a1, a2$. In the vicinity of the avoided crossings we find four states with nearly degenerate eigenenergies. Since all of those states correspond to regular phase-space parts, this process (which also increases the tunnelling rate around the avoided crossing) is different from chaos-assisted tunnelling. The existence of four nearly degenerate states implies the appearance of a new separatrix. Indeed, if

one of the two phase-space regions which support regular symmetry-breaking trajectories allows for the existence of a separatrix located completely inside this region, an image of this separatrix will appear in the second region on applying the symmetry operation. Two subregions separated inside the first region by the new separatrix will have two images in the other phase-space region. These four subregions can support tori which yield nearly degenerate eigenenergies.

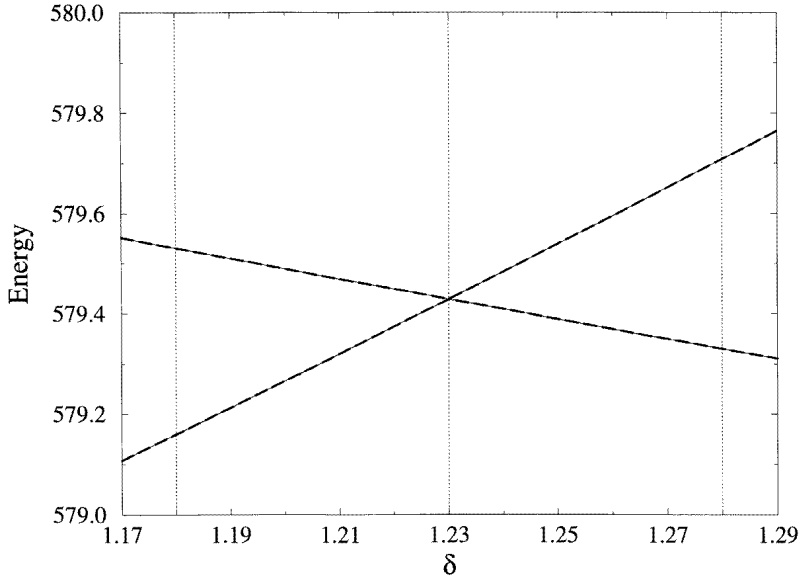

Figure 4. An enlargement of figure 2 to show a particular pair–pair interaction. Solid lines—symmetric eigenstates; thick dashed lines—antisymmetric eigenstates. The dotted lines mark the values of δ at which the eigenfunctions are analysed (see the following figures). The symmetric eigenstates have ordering numbers 413 and 414 (ordered with respect to increasing eigenenergy values).

In order to test these predictions, we analyse the details of an avoided crossing of two pairs. In figure 4 the eigenenergies are plotted in the vicinity of such an avoided crossing. In figures 5(a)–5(f) the densities $\rho(n, m)$ of the symmetric eigenstates $s1, s2$ are monitored as δ is varied through the avoided crossing. In figure 6 a Poincaré map of the classical phase-space flow is obtained for the avoided crossing parameters. First we do indeed observe an additional separatrix which is located completely inside the old symmetry-broken regions. Secondly the quantum densities $\rho(n, m)$ show a four-peak structure—two peaks per symmetry-broken region. The positions of the peaks correspond to the different subparts of both symmetry-broken regions, and both peaks inside one symmetry-broken region are separated by the additional separatrix.

4.3. Pair break-up

So far we have discussed avoided crossings which left the tunnelling pairs intact. Except for in a narrow parameter region around the avoided crossings (no matter whether they are pair–pair or single-state–pair ones), the tunnelling pairs recover after the crossing, and the transport of the eigenfunctions through the avoided crossing restores most of the details of the tunnelling states after the avoided crossing. So we can conclude that tunnelling

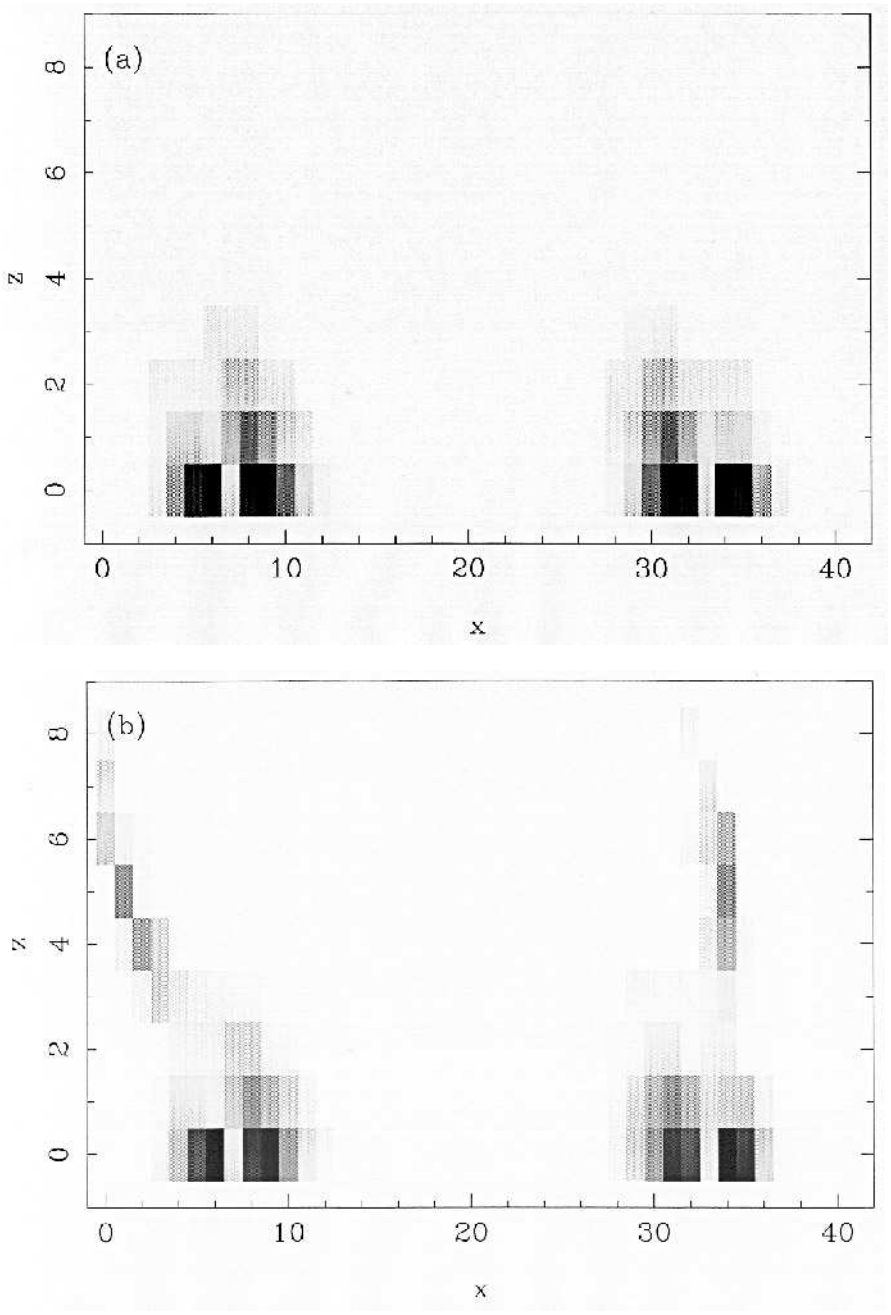

Figure 5. The densities of the symmetric eigenstates 413 and 414 are plotted in a greyscale representation (black—maximum values, white—minimum values) in the (x, z) plane (here x is the number of bosons on site 1, and z is the number of bosons on site 3). (a) 413, $\delta = 1.18$; (b) 413, $\delta = 1.23$; (c) 413, $\delta = 1.28$; (d) 414, $\delta = 1.18$; (e) 414, $\delta = 1.23$; (f) 414, $\delta = 1.28$.

pair eigenstates exist at least as long as there is enough regular phase space to support symmetry-broken classical trajectories.

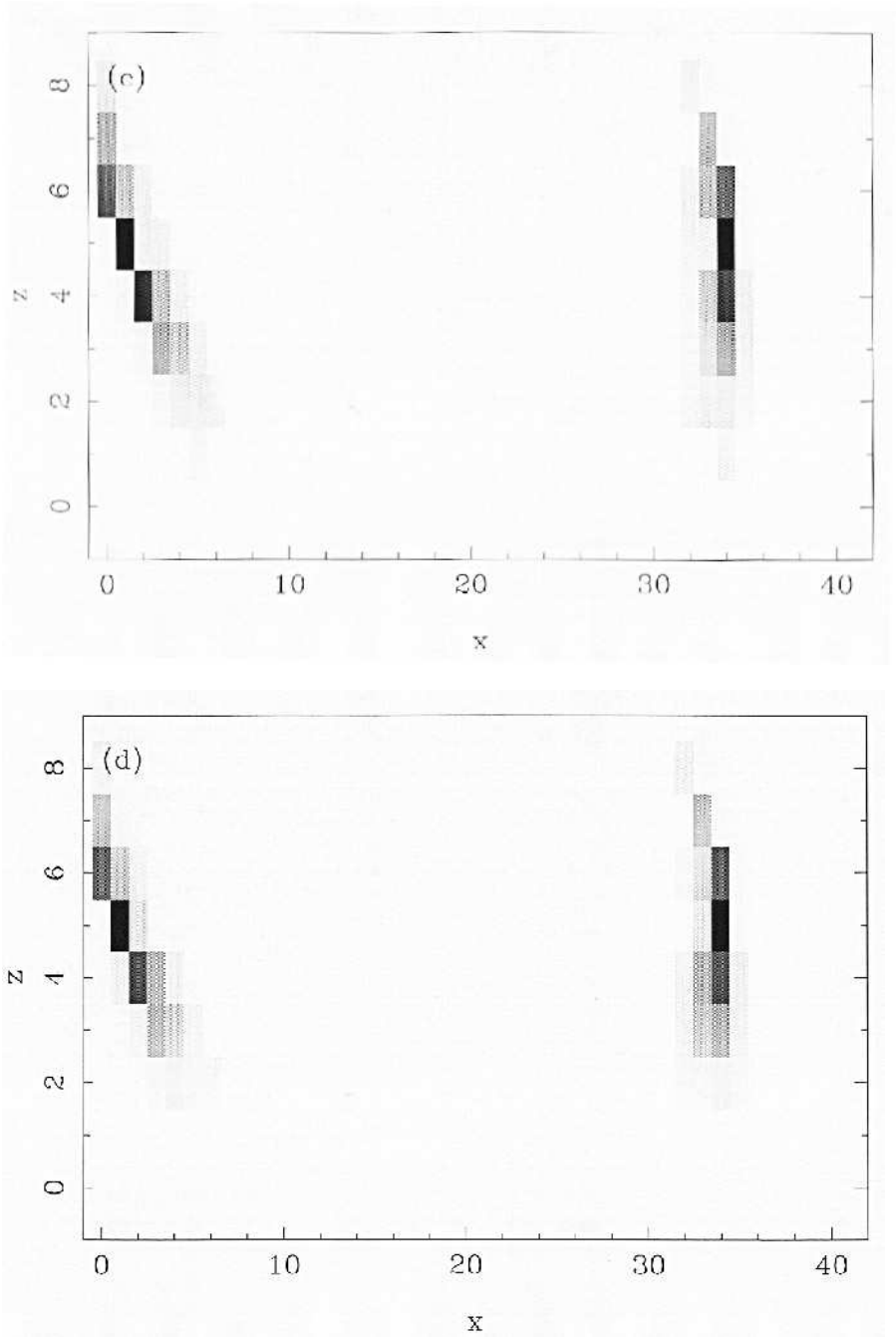

Figure 5. (Continued)

A break-up of a tunnelling pair is then a process which corresponds in the classical model to a chaotization of the phase space [40]. We observed many cases of break-up of a tunnelling pair upon variation of δ. The break-up is similar to an avoided crossing, but it is

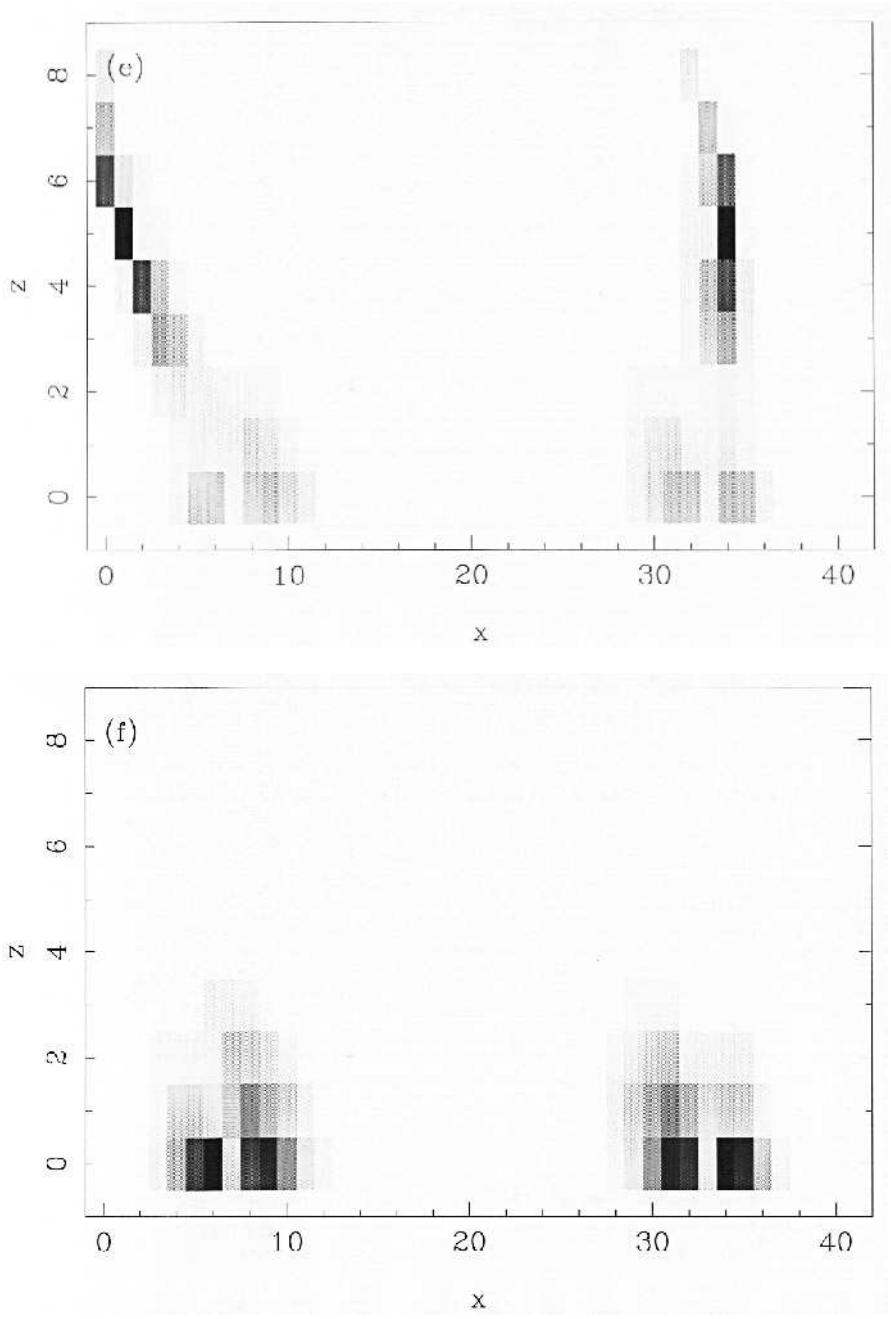

Figure 5. (Continued)

hard to say how many states participate. This is so because the energy distances between the pair and other states are not small compared to the average spacing. The densities of the associated states typically move into the classically chaotic region upon the break-up.

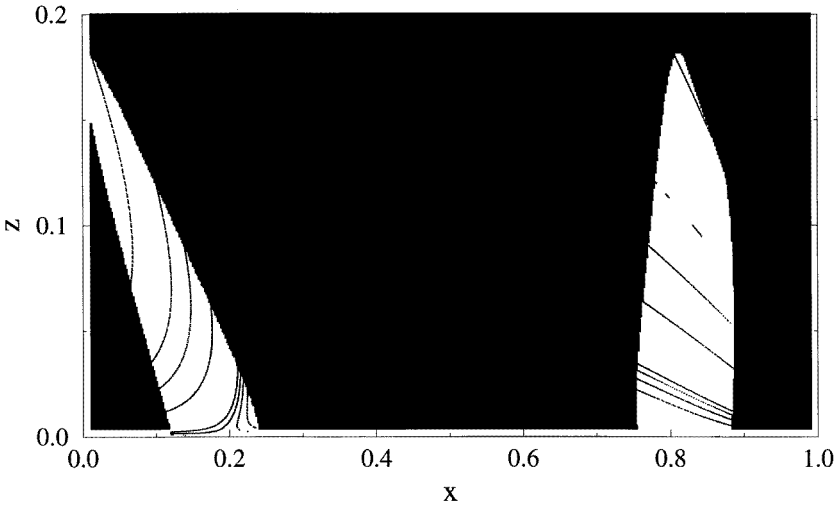

Figure 6. A Poincaré map of the classical phase-space flow of the trimer. The black area is forbidden. The map condition is $\Delta_{23} = 0$. The axes are $x = A_1^2$ and $z = A_3^2$. The parameters are $B = 1$, $C = 0.05$, $\delta = 0.030\,75$, and $E = 1.136\,2125$. These parameters correspond to the avoided crossing in figure 4.

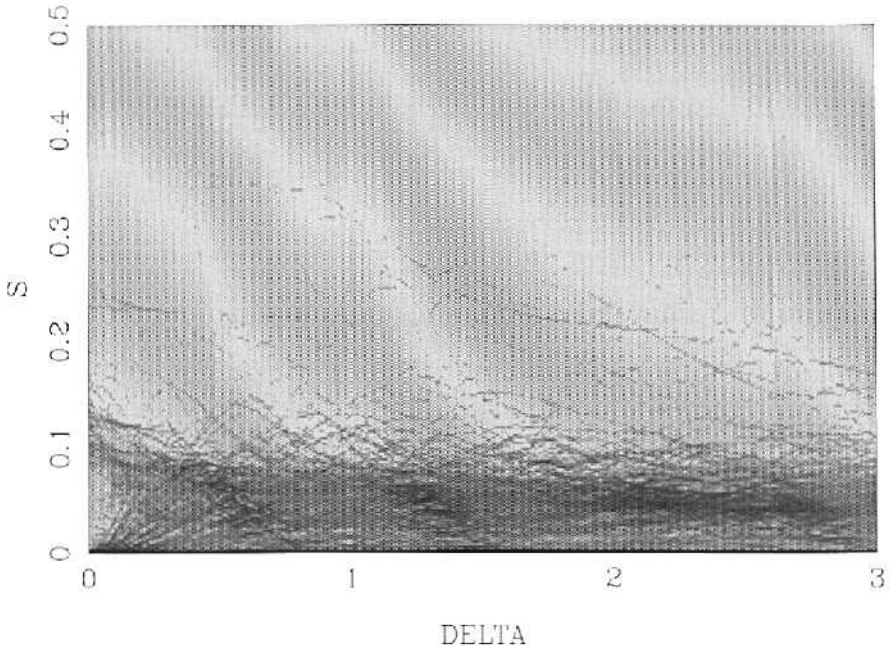

Figure 7. The logarithm of the distribution function of S for all of the symmetric eigenstates in a greyscale representation versus δ for the quantum trimer with $b = 40$ and $C = 2$. Note that the thick black line at the bottom represents all of the symmetric states with exponentially small values of S.

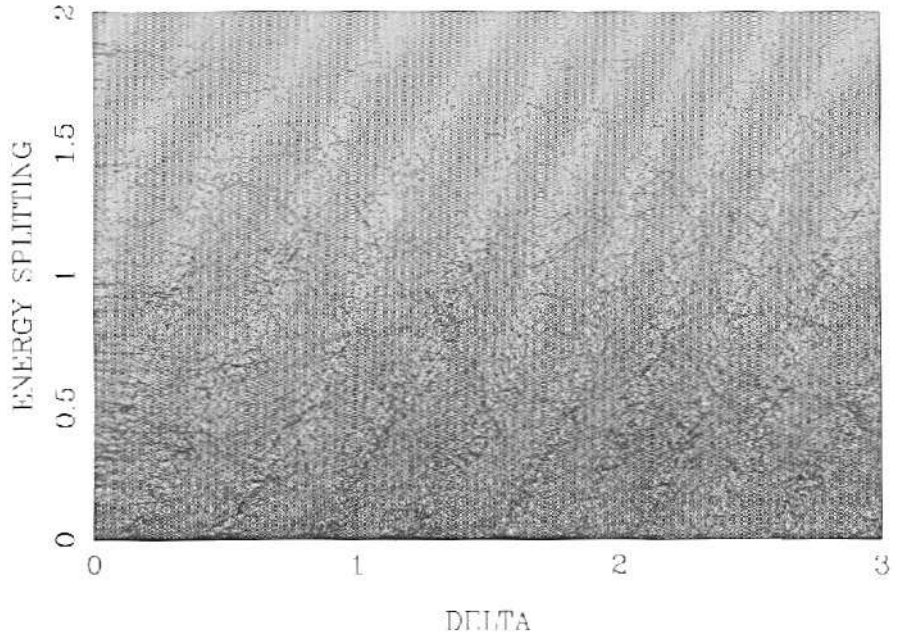

Figure 8. The distribution of the energy splittings versus δ in a greyscale representation for the quantum trimer with $b = 40$ and $C = 2$.

4.4. Statistical properties

To better characterize the properties of the system with respect to tunnelling pairs, we calculated the distribution functions. In figure 7 we plot the logarithm of the distribution function of the hyperbolic eigenfunction part S, and in figure 8 the distribution function for the energy splittings, with δ being an additional variable. We find that the number and density of tunnelling states changes smoothly as δ varies. This happens in spite of the fact that lots of avoided crossings occur. Consequently the existence of tunnelling pairs is predominantly due to the existence of regular phase-space structures which are not invariant under permutational symmetry. The existence of a chaotic layer, as well as the appearance of additional separatrices, does lead to fluctuations in the tunnelling splittings—but these fluctuations occur on energy scales small compared to the averaged spacing, and have no visible global impact on the statistics. The gradual increase of the chaotic phase-space part at the expense of the regular one leads to a smooth decrease in the number of tunnelling states.

5. Survival probability

In this section we want to discuss the relevance of our studies to the problem of intramolecular energy flow in molecules. This topic is a central one in the area of chemical physics (see review of Lehmann *et al* for details [49]). The problem is that of understanding the dynamical properties of energy flow from some initially excited states (say, some local bonds) to other states. Statistical theories of unimolecular reaction rates assume that the vibrational degrees of freedom rapidly exchange energy, where the density of states at a

given energy is the essential parameter. Recent experiments suggest that these theories are not applicable to a number of systems [49] (e.g. increase in the density of states by three orders of magnitude is accompanied by an *increase* of the excited state's lifetime by a factor of two!) The notion of the so-called *doorway states* is then stressed as a possible way out. These doorway states have to have strong weight with respect to the lifetime of excitations.

In the case of the trimer discussed here, we can demonstrate the effect of doorway states. A single-bond excitation in our case will correspond to placing a certain number of bosons on site one, and all of the rest (to end up with b bosons) on site three. Site two will remain empty. According to our notation such an initial state will be denoted by $|\Phi\rangle_{n0}$. Clearly such a state is not an eigenstate, so in the course of time it will 'spread', i.e. the excited eigenstates will evolve according to the time-dependent Schrödinger equation. Since the spectrum of the trimer for a given b is discrete, the time evolution of the initial state will be quasiperiodic. However, the total number of states for $b = 40$ is of the order of 10^3. This makes return probabilities small, in principle.

The survival probability of a given initial state

$$|\Psi\rangle_{n0} = \sum \phi_\mu^{n0} |\Psi\rangle_\mu$$

is defined in terms of the eigenstates $|\Psi\rangle_\mu$ with the eigenenergies E_μ as

$$P_u(t) = \sum_{\mu\mu'} I_\mu^{n0} I_{\mu'}^{n0} \mathrm{e}^{-\mathrm{i}(E_\mu - E'_\mu)t}$$

where

$$I_\mu^{n0} = |\phi_\mu^{n0}|^2$$

are the spectral intensities for the chosen initial state (see [15]). In figures 9(a) and 9(b) we plot both the spectrum and the survival probability for $n = 20$. The spectrum shows that about one hundred eigenstates are excited to form the initial state. However, the survival probability shows up with nearly periodically returning peaks. The returning probability is about 10%, and this means that the initial single-bond excitation is not dispersed completely. The explanation of the observed pattern is that doorway states carry a significant weight with respect to the returning probability of the initial excitation. These doorway states are the already discussed tunnelling pair states. A close analysis of the states involved in the spectrum in figure 9(a) shows that three tunnelling pairs contribute in the peak of the spectrum. These six states are dominant with respect to the return probability. The two energy distances between the three pairs define two frequencies. These frequencies precisely correspond to the two observed periods—one between the return probability pulses, and one between maxima within one return probability pulse. The exponentially small splittings within each pair define very large periods, inaccessible during the relatively short times of our observation in figure 9(b).

6. Discussion

In this paper we have discussed classical and quantum properties of the trimer with the aim of making progress in the understanding of quantum discrete breathers. We concentrated on the high-energy domain where correspondence between classical and quantum solutions should hold. The classical phase space supports trajectories violating the discrete symmetry of the system (here, the site permutation symmetry). The quantum eigenvalue problem yields corresponding pairs of tunnelling states. By tuning a single model parameter we can change the degree of chaotization of the classical phase space. This is reflected in the

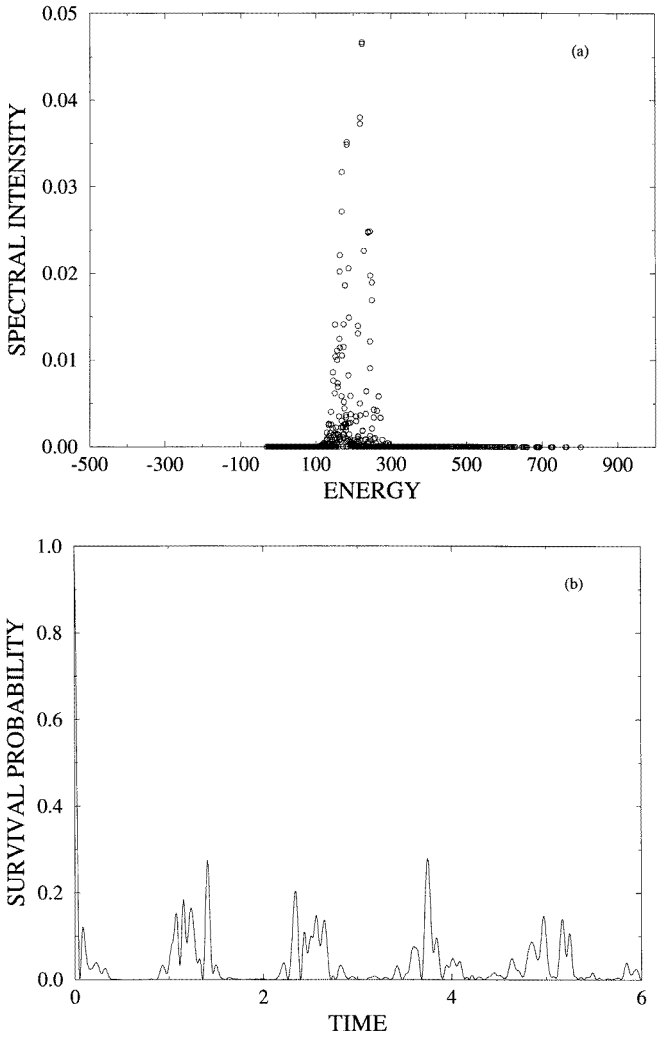

Figure 9. The survival probability of an initial state with 20 bosons on site 1 and 20 bosons on site 3. (a) The spectral intensity (open circles) is plotted versus eigenenergy. (b) The survival probability is plotted versus time. In both cases $b = 40$, $C = 2$, and $\delta = 1$.

behaviour of the tunnelling splittings. Avoided crossings between eigenvalues of pairs with eigenvalues of single states or other pairs are observed. While the first case corresponds to the so-called chaos-assisted tunnelling (the single state corresponds to chaotic phase-space parts), the second one indicates the appearance of additional separatrix structures on finer scales in the classical phase space. Neither case leads to a disappearance of the tunnelling state. The wave functions are 'transported' through the avoided crossings, and are recovered once the avoided crossing is passed. A break-up of a tunnelling state is observed if the corresponding classical phase-space part ceases to support regular trajectories.

From the above, we could conclude that quantum breather states should exist in the high-energy domain of a given model, if there is enough regular support from the phase-space parts surrounding families of classical discrete breather orbits. However, the trimer

considered by us lacks one important property of generic classical Hamiltonian systems with a larger number of degrees of freedom—namely, the existence of the Arnold web, which connects all chaotic phase-space parts [50]. Instead, the low dimensionality of the relevant phase space of the trimer (effectively two degrees of freedom) leads to the topological effect of trapping of chaotic layers between invariant tori. What is the effect of the Arnold web? Essentially it sets a second timescale, which depends on the details of the system, and mainly on its distance from an integrable system. This timescale determines how long a trajectory, launched in a chaotic layer near to a regular trajectory, will evolve close to the regular trajectory. For larger times a diffusive-like process transports the trajectory to other parts of the Arnold web. This timescale is related to the largest Lyapunov coefficient. The Nekhoroshev theorems provide analytical estimates for these timescales [51].

An important thing to notice is that classical discrete breathers have finite energies. For a large system one could argue that the energy density is small, and thus the phase-space flow considered is nearly regular. This is not so, because the discrete breather solutions are localized in space. Consequently the energy density is finite, but only in a finite volume. In order to understand the dynamics of trajectories close to the discrete breather orbits we could then conclude that it would be enough to restrict ourselves to a low-dimensional phase space (which, however, should still exhibit an Arnold web). It, thus, remains as an interesting task to study the effect of this Arnold web on tunnelling states in the high-energy domain. The problem is nontrivial, because some arguments relate quantum mechanics in the high-energy domain to boxing of the classical phase space and subsequent averaging over classical dynamics in the box. High energies or the classical limit corresponds then to a decrease of the box size. In the absence of Arnold webs this seems not to be important, since thin chaotic layers are constrained between tori. However, in the presence of an Arnold web things might change. A certain box might be large enough not to be influenced by fine web structures, and the quantum state could correspond to a regular trajectory. Decreasing the box size, we effectively enlarge the classical phase space, and the sensitivity to chaotic parts may increase.

We have also shown that the concept of doorway states in the problem of single-bond excitations of molecules can be directly related to tunnelling, and thus to classical trajectories which are not invariant under certain discrete symmetries (when the Hamiltonian is).

Finally we want to stress that the trimer model used here is easy to apply for numerical diagonalizations (of the quantum problem). It can be thus of benefit for studies of the general topics in quantum chaos.

Acknowledgments

We thank S Aubry, T Dittrich, C Eilbeck and K Müller for helpful discussions, and P Fulde for continuous interest. SF thanks the Physics department of Tel Aviv University for hospitality during a stay when part of this work was done. VF thanks the Max-Planck-Institute for Physics of Complex Systems for hospitality during two stays, when part of this work was done.

References

[1] Kosevich A M and Kovalev A S 1974 Selflocalization of vibrations in a one-dimensional anharmonic chain *Sov. Phys.–JETP* **67** 1793

[2] Takeno S, Kisoda K and Sievers A J 1988 Intrinsic localized vibrational modes in anharmonic crystals *Prog. Theor. Phys. Suppl.* **94** 242

[3] Sievers A J and Page J B 1995 Unusual anharmonic local mode systems *Phonon Physics—The Cutting Edge (Dynamical Properties of Solids VII)* ed G K Horton and A A Maradudin (Amsterdam: Elsevier) p 137
[4] Flach S, Willis C R and Olbrich E 1994 Integrability and localized excitations in nonlinear discrete systems *Phys. Rev.* E **49** 836
[5] Flach S and Willis C R 1994 Movability of localized excitations in nonlinear discrete systems *Phys. Rev. Lett.* **72** 1777
[6] Flach S, Kladko K and Willis C R 1994 Localized excitations in two-dimensional lattices *Phys. Rev.* E **50** 2293
[7] Flach S 1994 Conditions on the existence of localized excitations in nonlinear discrete systems *Phys. Rev.* E **50** 3134
[8] MacKay R S and Aubry S 1994 Proof of existence of breathers for time-reversible or hamiltonian networks of weakly coupled oscillators *Nonlinearity* **7** 1623
[9] Flach S 1995 Existence of localized excitations in nonlinear hamiltonian lattices *Phys. Rev.* E **51** 1503
[10] Flach S 1995 Obtaining breathers in nonlinear hamiltonian lattices *Phys. Rev.* E **51** 3579
[11] Flach S 1996 Tangent bifurcation of band edge plane waves, dynamical symmetry breaking and vibrational localization *Physica* D **91** 223
[12] Flach S and Kladko K 1996 Interaction of discrete breathers with electrons in nonlinear lattices *Phys. Rev.* B **53** 11 531
[13] Bogdan M M and Kosevich A M 1976 Quantization of self-localized vibrations in a one-dimensional anharmonic chain *Sov. J. Low Temp. Phys.* **2** 391
[14] Wang W Z, Tinka Gammel J, Bishop A R and Salkola M I 1996 Quantum breathers in a nonlinear lattice *Phys. Rev. Lett.* **76** 3598
[15] Schofield S A, Wyatt R E and Wolynes P G 1996 Computational study of many-dimensional quantum vibrational energy redistribution *J. Chem. Phys.* **105** 940
[16] Miller P D, Scott A C, Carr J and Eilbeck J C 1991 Binding energies for discrete nonlinear Schrödinger equations *Phys. Scr.* **44** 509
[17] Scott A C, Eilbeck J C and Gilhøj H 1994 Quantum lattice solitons *Physica* D **78** 194
[18] Bernstein L, Eilbeck J C and Scott A C 1990 The quantum theory of local modes in a coupled system of nonlinear oscillators *Nonlinearity* **3** 293
[19] Bernstein L J 1993 Quantizing a self-trapping equation *Physica* D **68** 174
[20] Aubry S, Flach S, Kladko K and Olbrich E 1996 Manifestation of classical bifurcation in the spectrum of the integrable quantum dimer *Phys. Rev. Lett.* **76** 1607
[21] Eilbeck J C, Lomdahl P S and Scott A C 1985 The discrete self-trapping equation *Physica* D **16** 318
[22] Hennig D, Gabriel H, Jørgensen M F, Christiansen P L and Clausen C B 1995 Homoclinic chaos in the discrete self-trapping trimer *Phys. Rev.* E **51** 2870
[23] De Filippo S, Fusco G M and Salerno M 1989 *Nonlinearity* **2** 477
[24] Chefles A 1996 Nearest-neighbour level spacings for the non-periodic discrete nonlinear Schrödinger equation *J. Phys. A: Math. Gen.* **29** 4515
[25] Cruzeiro-Hansson L, Feddersen H, Flesch R, Christiansen P L, Salerno M and Scott A C 1990 Classical and quantum analysis of chaos in the discrete self-trapping equation *Phys. Rev.* B **42** 522
[26] Feddersen H, Christiansen P L and Salerno M 1991 Quantum chaology in the discrete self-trapping equation in the presence of Arnold diffusion *Phys. Scr.* **43** 353
[27] Wright E, Eilbeck J C, Hays M H, Miller P D and Scott A C 1993 The quantum discrete self-trapping equation in the Hartree approximation *Physica* D **69** 18
[28] Gutzwiller M C 1990 *Chaos in Classical and Quantum Mechanics* (Berlin: Springer)
[29] Auerbach A, Kivelson S and Nicole D 1984 Path decomposition for multidimensional tunneling *Phys. Rev. Lett.* **53** 411
[30] Wilkinson M 1986 Tunneling between tori in phase space *Physica* D **21** 341
[31] Wilkinson M and Hannay J H 1987 Multidimensional tunneling between excited states *Physica* D **27** 201
[32] Huang Z H, Feuchtwang T E, Cutler P H and Kazes E 1990 Wentzel–Kramers–Brillouin method in multidimensional tunneling *Phys. Rev.* A **41** 32
[33] Creagh S C 1994 Tunnelling in multidimensional systems *J. Phys. A: Math. Gen.* **27** 4969
[34] Aubry S 1997 Breathers in nonlinear lattices: existence, linear stability and quantization *Physica* D **103** 201
[35] Bohigas O, Tomsovic S and Ullmo D 1993 Manifestations of classical phase space structures in quantum mechanics *Phys. Rep.* **223** 43
[36] Davis M J and Heller E J 1986 Quantum dynamical tunneling in bound states *J. Chem. Phys.* **75** 246
[37] Bohigas O, Tomsovic S and Ullmo D 1990 Dynamical quasidegeneracies and separation of regular and irregular quantum levels *Phys. Rev. Lett.* **64** 1479

[38] Lin W A and Ballentine L E 1990 Quantum tunneling and chaos in a driven anharmonic oscillator *Phys. Rev. Lett.* **65** 2927
[39] Roncaglia R, Bonci L, Izrailev F M, West B J and Grigolini P 1994 Tunneling versus chaos in the kicked Harper model *Phys. Rev. Lett.* **73** 802
[40] Utermann R, Dittrich T and Hänggi P 1994 Tunneling and the onset of chaos in a driven bistable system *Phys. Rev.* E **49** 273
[41] Yukawa T 1985 New approach to the statistical properties of energy levels *Phys. Rev. Lett.* **54** 1883
[42] Nakamura K and Lakshmanan M 1986 Complete integrability in a quantum description of chaotic systems *Phys. Rev. Lett.* **57** 1661
[43] Wilkinson M 1987 Narrowly avoided crossings *J. Phys. A: Math. Gen.* **20** 635
[44] Wilkinson M and Austin E J 1993 Densities of degeneracies and near-degeneracies *Phys. Rev.* A **47** 2601
[45] von Neumann J and Wigner E P 1929 *Phys. Z.* **30** 467
[46] Landau L D and Lifshitz E M 1991 *Quantenmechanik (Lehrbuch der Theoretischen Physik III)* (Berlin: Akademie)
[47] Berry M V 1984 Quantal phase factors accompanying adiabatic changes *Proc. R. Soc.* A **392** 45
[48] Hillery M, O'Connell R F, Scully M and Wigner E P 1984 *Phys. Rep.* **106** 121
[49] Lehmann K K, Scoles G and Pate B H 1994 Intramolecular dynamics from eigenstate-resolved infrared spectra *Annu. Rev. Phys. Chem.* **45** 241
[50] Sagdeev R S, Usikov D A and Zaslavski G M 1988 *Nonlinear Physics: from the Pendulum to Turbulence and Chaos* (New York: Harwood Academic)
[51] Nekhoroshev N N 1977 An exponential estimate of the time of stability of nearly-integrable Hamiltonian systems *Russ. Math. Survey* **32** 1